ChemComm

Iron Homo- and Heterobimetallic Complexes Supported by a Symmetrical Dinucleating Ligand

Journal:	*ChemComm*
Manuscript ID	CC-COM-05-2024-002155.R1
Article Type:	Communication

COMMUNICATION

Iron Homo- and Heterobimetallic Complexes Supported by a Symmetrical Dinucleating Ligand

Received 00th January 20xx,
Accepted 00th January 20xx

DOI: 10.1039/x0xx00000x

Pablo Ríos,‡[a,b] Matthew S. See,‡[b,c] Oscar Gonzalez,[b] Rex C. Handford,[b] Amélie Nicolay,[b,c] Guodong Rao,[d] R. David Britt,*[d] D. Kwabena Bediako,*[b] and T. Don Tilley*[b,c]

The selective synthesis of biomimetic Fe/Mn complexes able to mimic the geometry and catalytic activity of enzymes possessing this cofactor is still a challenge. Herein, we discuss the stepwise synthesis, characterization, and magnetic properties of a Fe(II)/Mn(II) species and related Fe(II)/Fe(II) complexes.

The participation of two metals in the active site of enzymes allows for the chemical functionalization of kinetically inert substrates (*e.g.* aerobic oxidation of strong, aliphatic C–H bonds) under mild conditions. Representative examples include homo- (Fe/Fe) and heterobimetallic (Fe/Mn) cofactors, as in soluble methane monooxygenase (sMMO)[1] or 2-aminoisobutyric acid hydroxylase,[2] respectively (Figure 1A). While the environment created by the tertiary structure of proteins facilitates assembly of the dinuclear active site, the incorporation of heterobimetallic cores requires metal differentiation through selective binding of the amino acid residues to each of the metal centers. In the case of Fe(II) and Mn(II), their comparable radii[3] and coordination preferences[4] make this differentiation a challenging task. From the molecular synthetic viewpoint, the construction of Fe/Mn models requires an appropriate strategy that employs a favorable coordination environment for the binuclear site of interest. For this purpose, a number of research groups have utilized unsymmetrical ligands. With differentiated binding sites, selective formation of a heterobimetallic core can be achieved.[5] This strategy has been used by this laboratory in the synthesis of Cu-based 1st-row transition metal heterobimetallic complexes.[6,7] However, symmetrical ligands are also capable of binding Fe and Mn in close contact (Figure 1B), as illustrated by different approaches that have been reported. Que and coworkers observed the self-assembly of Fe(III)/Mn(II) species by sequential addition of the metal precursors to a solution of the 2,6-bis[(bis(2-pyridylmethyl)amino)methyl]-4-methylphenol ligand.[8] In a similar manner, the group of Zhang selectively synthesized an Fe(II)/Mn(II) complex utilizing a symmetrical dimercaptan-1,3,4-thiadiazole scaffold.[9] The metal differentiation, in this case, is attributed to the unsymmetrical binding of a coordinated carboxylate ligand. On the other hand, Wieghardt and Girerd, *et al.* obtained a heterobimetallic Fe(III)/Mn(III) complex by hydrolysis of a 1:1 mixture of $LFeCl_3$ and $L'MnCl_3$ (L and L' = 1,4,7-triazacyclononane-derived ligands) in the presence of sodium acetate.[10] Related Fe(III)/Mn(IV) systems containing TACN ligands have also been described by Borovik *et al.*[11] Herein, we report the stepwise synthesis of an Fe(II)/Mn(II) complex utilizing a bioinspired, symmetrical 1,8-naphthyridine-based ligand. The isolation of a monometallic Fe(II) species with an empty, neighboring binding site provided the opportunity to subsequently add a second metal center such as Mn(II).

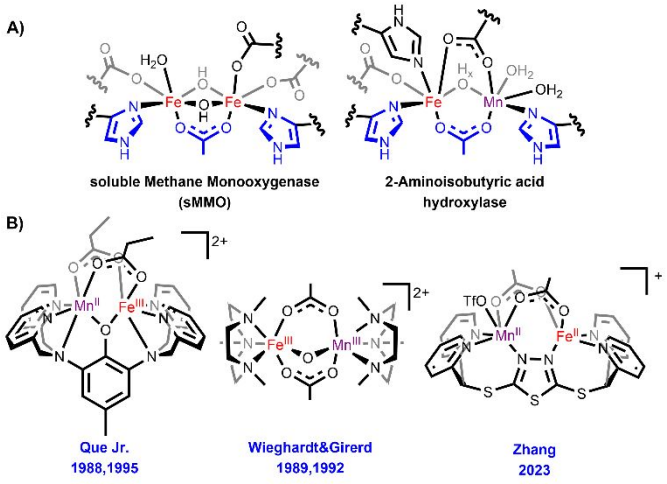

Figure 1. Examples of (A) Fe-containing homo- and heterobimetallic cofactors for aerobic C–H oxidation and (B) Previously reported synthetic Fe/Mn complexes with symmetrical ligands.

[a] *Instituto de Investigaciones Químicas (IIQ), Departamento de Química Inorgánica, Centro de Innovación en Química Avanzada (ORFEO-CINQA), CSIC and Universidad de Sevilla, 41092 Sevilla, Spain*
[b] *Department of Chemistry, University of California Berkeley (USA)*
[c] *Chemical Sciences Division, Lawrence Berkeley National Laboratory, Berkeley, CA 94720 USA*
[d] *Department of Chemistry, University of California, Davis, Davis, California 95616, United States*
‡*Both authors contributed equally to this work.*

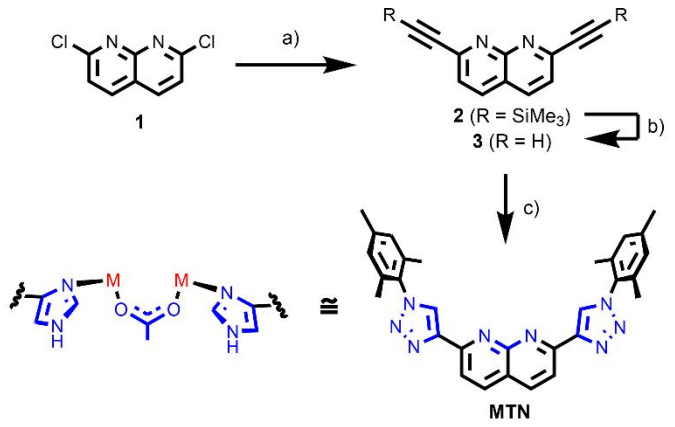

Scheme 1. Reaction conditions and isolated yields: a) Me_3SiCCH (2.2 equiv.), $Pd(PPh_3)_2Cl_2$ (0.5 mol%), CuI (0.5 mol%), Et_3N (20 equiv.), THF, 65 °C, 21 h, 72%. b) K_2CO_3 (1.4 equiv.), $MeOH/CH_2Cl_2$ 1:1, 23 °C, 30 min, 85%. c) Mesityl azide (2.1 equiv.), $CuSO_4$ (10 mol%), L-sodium ascorbate (0.8 equiv.), $EtOH/H_2O$ 1.25:1, 60 °C, 20 h, 93%.

Structural analysis of homo- and heterobimetallic enzymatic cofactors reveals recurrent patterns, such as imidazole rings from histidine residues binding single metal atoms, or carboxylate groups with a *syn, syn* coordination mode acting as bridging ligands between both metal centers (Figure 1A, blue fragments).[1,2] Based on these structural motifs, and taking into consideration Lippard's 1,8-naphthyridine/masked carboxylate analogy,[12] ligand MTN (2,7-bis(1-**M**esityl-1*H*-1,2,3-**T**riazol-4-yl)-1,8-**N**aphthyridine) was envisaged as an easily accessible target (Scheme 1). Indeed, 2,7-dichloronaphthyridine reacted with trimethylsilylacetylene under Sonogashira coupling conditions to give **2** in 72% yield.[13] Desilylation gave 2,7-diethynyl-1,8-naphthyridine **3**, which was subjected to Cu(I)-catalyzed 1,3-dipolar cycloaddition with mesityl azide to incorporate the 1,4-substituted triazole units onto the 1,8-naphthyridine scaffold in 93% yield. Single crystal X-ray analysis displays the triazole arrangement depicted in Scheme 1 (Figure S17), with the nitrogen atoms pointing away from the binding site. Nonetheless, relaxed potential energy surface scan calculations indicate that rotation of the triazole fragment requires 8.1 kcal mol^{-1} (Figure S23), which suggests that chelation through the side-arms is experimentally possible. Initial metalation studies involved the addition of a mixture of $FeCl_2$ and $Fe(NTf_2)_2$ to a THF solution of MTN in a 1:1:1 ratio, in order to obtain a cationic diiron complex possessing two bridging chloride ligands. However, X-ray diffraction analysis on single crystals grown from a THF/hexane bilayer revealed the stoichiometry $[(MTN)_2Fe_2(\mu\text{-}Cl)(THF)_2][NTf_2]_3$ (**4**, Figure 2 and Scheme 2).

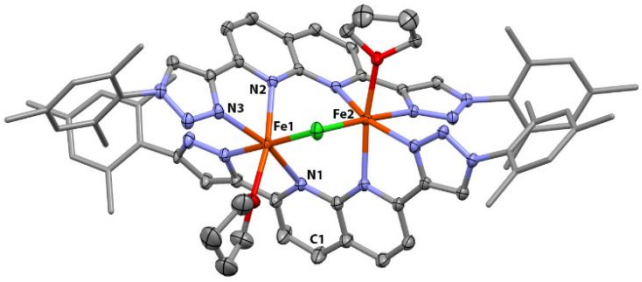

Figure 2. Solid-state molecular structure of **4** (50% probability ellipsoids). H atoms and bis(trifluoromethylsulfonyl)imide (NTf_2) anions omitted and mesityl groups represented as capped sticks for clarity.

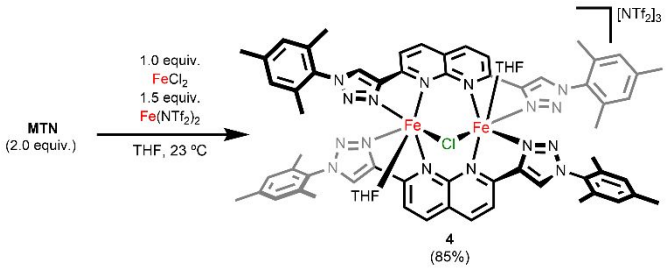

Scheme 2. Synthesis of complex **4** (isolated yield in parenthesis).

Each Fe(II) center is bound to one naphthyridine nitrogen and its adjacent triazole side-arm. There are two MTN molecules in the structure, presumably due to the tendency of the Fe(II) centers to adopt the observed distorted octahedral geometry (*e.g.* ∠N1–Fe1–N3 = 158.3(7)°). The rest of the coordination sphere of each metal is completed by a THF molecule and a chloride ligand that bridges both metals (∠Fe1–Cl–Fe2 = 90.3(3)°, Fe···Fe = 3.380(5) Å). A remarkable geometrical feature of this complex is the deviation of the Fe atoms from the naphthyridine planes (*e.g.* ∠C1–N1–Fe1 = 156.3(1)°). A spacefill representation of the solid-state structure suggests that the steric congestion provided by the mesityl rings is responsible for the observed structural distortion (Figure S22).

Based on the X-ray diffraction data, the stoichiometry of the reagents was adjusted (2 equiv. of MTN, 1.5 equiv. of $Fe(NTf_2)_2$ and 1 equiv. of $FeCl_2$) to optimize the synthesis of complex **4** (Scheme 2), which under these conditions was obtained in 85% yield as analytically pure orange crystals. Notably, while optimizing the reaction conditions, the formation of pink crystals was observed upon crystallization when $FeCl_2$ was added in excess relative to $Fe(NTf_2)_2$. Unlike **4**, these crystals remained insoluble in THF and other common organic solvents like MeCN, CH_2Cl_2 or acetone. Interestingly, analysis of the single crystal X-ray diffraction data reveals formation of the monometallic species $MTN{\cdot}FeCl_2$ (**5,** Figure 3, top). The solid-state structure of **5** exhibits an iron center with a distorted tetrahedral geometry (τ_4 value[14]

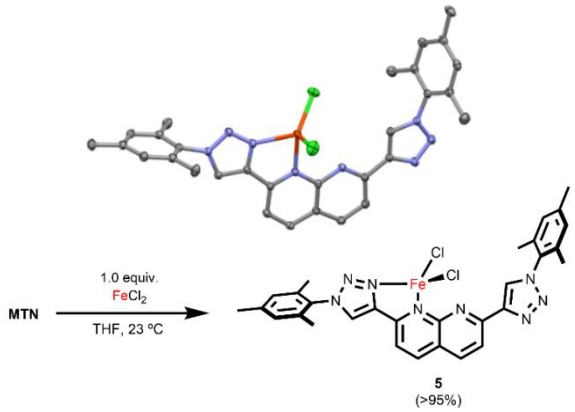

Figure 3. Top: Solid-state molecular structure of **5** (50% probability ellipsoids). H atoms omitted for clarity. **Bottom**: Synthesis of complex **5** (isolated yield in parenthesis).

of 0.87) bound to two chloride ligands, one triazole side-arm and one of the naphthyridine nitrogen atoms. The other half of the MTN ligand remains available for coordination of a second metal, which makes **5** a potential platform to access heterobimetallic complexes.

The selective synthesis of **5** was targeted (Figure 3, bottom), with stirring a 1:1 mixture of MTN and $FeCl_2$ in THF at 23 °C for 22 h. This led to quantitative (>95% yield) precipitation of the pink solid, and combustion analysis (see Supporting Information) and effective magnetic moment measurements (μ_{eff} = 4.9 μ_B, Evans method, DMSO, 500 MHz) are in agreement with the observed solid-state structure.

From complex **5**, the formation of an Fe/Mn species was observed by addition of $Mn(OTf)_2$·3MeCN (1 equiv.). This reaction in MeCN solvent occurred over 2 h at 23 °C, to afford an orange solution, which yielded crystals after layering with diethyl ether. X-ray diffraction data revealed the product as having the formula $[(MTN)_3Fe(\mu\text{-}Cl)_2Mn][OTf_2]_2$ (**6**), with one MTN ligand binding both metals that are linked by two bridging chloride ligands (Figure 4). Moreover, the coordination sphere of each metal center is completed by an additional MTN unit, bound through one naphthyridine nitrogen and its adjacent triazole side-arm. Each metal adopts a highly distorted octahedral geometry (*e.g.* ∠N1–Fe–N2 or ∠N3–Mn–N4 ≈ 145°) as a consequence of the steric hindrance provided by the three MTN ligands. Optimizing the stoichiometry (*i.e.* 1 equiv. of **5**, 2 equiv. of MTN and 1 equiv. of $Mn(OTf)_2(MeCN)_3$) allowed for the selective formation of **6**, isolated as analytically pure orange crystals in 81% yield (Scheme 3). As expected, the similar electron densities of the metals make their distinction *via* X-ray diffraction difficult. Nonetheless, high-resolution mass spectra of such crystals dissolved in MeCN only exhibit a parent ion peak of the m/z ratio and isotope distribution pattern corresponding to **6** (Figures S13-S14), with no appreciable scrambling in solution that could give rise to a potential Fe/Fe or Mn/Mn species (see Supporting Information). Furthermore, EPR analysis of a frozen sample of **6** in ethanol reveals signals typical of an $S = 5/2$ Mn^{2+} ion (Figure 5 and Figures S24-S26), supporting the presence of Mn(II), the heterobimetallic assignment and the absence of exchange interactions between Mn(II) and Fe(II).

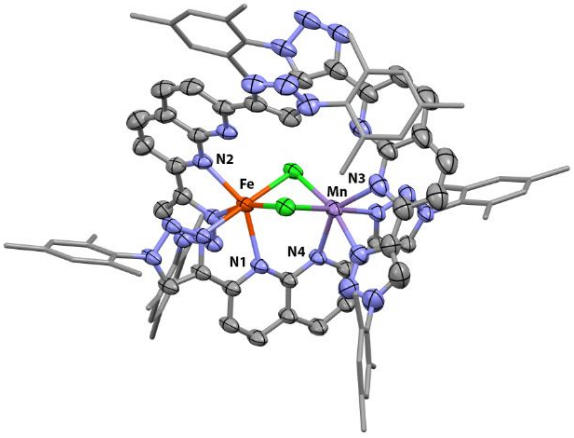

Figure 4. Solid-state molecular structure of **6** (50% probability ellipsoids). H atoms and (trifluoromethylsulfonate (OTf) anions omitted and mesityl groups represented as capped sticks for clarity.

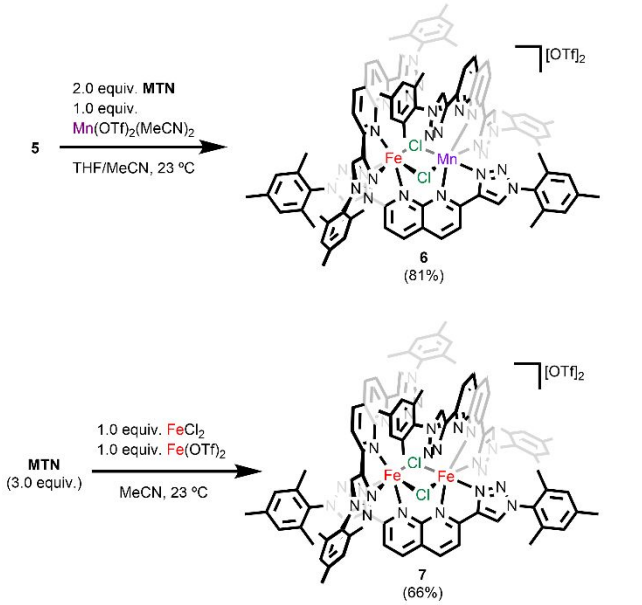

Scheme 3. Synthesis of complexes **6** and **7** (isolated yields in parentheses).

Interestingly, the nature of the weakly coordinating anion in the iron precursor appears to determine the number of MTN molecules in the final product (*i.e.* two MTN ligands in **4** in the case of NTf_2^- *vs* three MTN ligands in **6** for OTf^-). This hypothesis finds additional support in the synthesis of complex **7**, synthesized by adding a suspension of MTN (3 equiv.) in MeCN to a 1:1 mixture of $FeCl_2$ and $Fe(OTf)_2$. Complex **7** was isolated as red-orange crystals in 66% yield, and exhibits a solid-state structure that is essentially identical to that of the cationic fragment of complex **6** (Figures S20-S21). High-resolution mass spectrometry analysis of this sample displays a parent ion peak of the expected m/z and isotope distribution pattern, which is not present in the mass spectrum of complex **6** (Figures S15-16).

Variable-temperature magnetic susceptibility measurements of the bimetallic complexes **4**, **6**, and **7** were conducted under an applied DC field of 1 T.[15] The χT values for **6** and **7** increase as the temperature increases (Figure S27), which suggests the thermal population of higher spin states. Notably, the χT values of complex **7** increase slightly upon lowering the temperature, reaching a maximum value of 6.12 emu K Oe^{-1} mol^{-1} at approximately 78 K. This value of χT is consistent with two noninteracting S = 2 spins when g = 2. Furthermore, the Curie-Weiss law was used to fit magnetic susceptibility data to extract the Curie constant (related to the number of unpaired electrons) and the Curie-Weiss temperature (related to the strength of the molecular field) as shown in Figure S28. We find that the respective μ_{eff} values for **4**, **6**, and **7** are 6.55, 6.79, and 6.36 μ_B, which compare favorably to the expected spin-only calculations for μ_{eff}, which are 6.93, 7.68, and 6.93 μ_B, respectively. The difference between calculated and observed values may be rooted in the distorted octahedral environment of these systems as well as the underlying magnetic ordering. The Curie-Weiss temperatures (θ_{CW}) were determined to be -7.8, -20.9, and 11.6 K for **4**, **6**, and **7**, respectively. The Curie-Weiss temperatures for **4** and **6** are consistent with antiferromagnetic interactions, whereas the

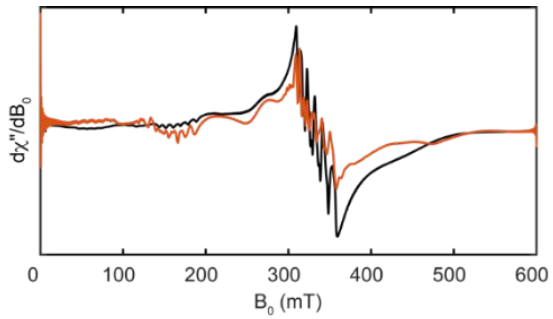

Figure 5. X-band EPR spectrum of **6** (10K, 0.2 mW) with simulation shown in red. Simulation parameters: S = 5/2, g = 1.98, A 55Mn = 250 MHz, D = 1900 MHz, E/D = 0.25.

Curie-Weiss temperature of **7** is emblematic of ferromagnetic interactions. Thus, by considering the discrepancies in magnetic susceptibility behavior from the prototypical complex given by **7**, we can determine that a change in the identity of the metal center (**6**), and the ligand field environment (**4**) can both lead to varied magnetic behavior given the particular exchange pathway of these materials.

In conclusion, the results above indicate that the selective synthesis of an Fe/Mn species utilizing a symmetrical dinucleating ligand can be carried out through a stepwise process involving isolation of the monometallic Fe(II) complex, followed by addition of Mn(II). In addition, the information extracted from variable-temperature magnetic susceptibility measurements suggest superexchange as a possible electronic property for these complexes, given that in these species the metal centers are separated by ligands. The possibility of superexchange as the predominant mechanism for magnetism opens routes to a variety of possible ferro- and antiferro-magnetic complexes within this ligand scaffold. Future research will focus on possible variations in the structure of this bimetallic system, including the nature of bridging ligands and the resulting influence on electronic and chemical properties.

This work was funded by the US Department of Energy, Office of Science, Office of Basic Energy Sciences, Chemical Sciences, Geosciences, and Biosciences Division under Contract no. DE-AC02-05CH11231. P. R. acknowledges funding from the European Union's Horizon 2020 research and innovation programme under the Marie Skłodowska-Curie grant agreement No. 841154. This research used resources of the Advanced Light Source, which is a DOE Office of Science User Facility under contract no. DE-AC02-05CH11231. We acknowledge the National Institutes of Health for funding the UC Berkeley College of Chemistry NMR facility, and the UC Berkeley Molecular Graphics and Computation Facility. EPR spectroscopy was supported by National Institutes of Health grant 2R35GM126961 (R.D.B.). We also acknowledge Magan M. Powell for helpful discussion about EPR spectroscopy.

Data availability

The data supporting this article have been included as part of the Supplementary Information.

Conflicts of interest

There are no conflicts to declare.

Notes and references

1 M. O. Ross and A. C. Rosenzweig, *J. Biol. Inorg. Chem.,* 2017, **22**, 307.
2 M. M. Powell, G. Rao, R. D. Britt and J. Rittle, *J. Am. Chem. Soc.,* 2023, **145**, 16526. Other selected Fe/Mn examples include: a) L. M. K. Dassama, C. Krebs, J. M. Bollinger, Jr., A. C. Rosenzweig, A. K. Boal, *Biochemistry*, **2013**, *52*, 6424. b) Y. Kutin, V. Srinivas, M. Fritz, R. Kositzki, H. S. Shafaat, J. Birrell, E. Bill, M. Haumann, W. Lubitz, M. Högbom, J. J. Griese, N. Cox, *J. Inorg. Biochem.,* **2016**, *162*, 164. c) O. M. Manley, H. N. Phan, A. K. Stewart, D. A. Mosley, S. Xue, L. Cha, H. Bai, V. C. Lightfoot, P. A. Rucker, L. Collins, T. I. Williams, W-C. Chang, Y. Guo, T. M. Makris, *Proc. Natl. Acad. Sci. U. S. A.* **2022**, *119*, e2210908119. d) C. Liu, M. M. Powell, G. Rao, R. D. Britt, J. Rittle, *J. Am. Chem. Soc.* **2024**, *146*, 1783.
3 a) B. Cordero, V. Gómez, A. E. Platero-Prats, M. Revés, J. Echeverría, E. Cremades, F. Barragán and S. Alvarez, *Dalton Trans.,* 2008, 2832-2838. b) R. D. Shannon, *Acta Cryst.,* 1976, **A32**, 751.
4 a) J. A. Cotruvo Jr. and J. Stubbe, *Metallomics,* 2012, **4**, 1020. b) J. J. Griese, K. Roos, N. Cox, H. S. Shafaat, R. M. M. Branca, J. Lehtiö, A. Gräslund, W. Lubitz, P. E. M. Siegbahn and M. Högbom, *Proc. Natl. Acad. Sci. U. S. A.,* 2013, **110**, 17189.
5 Some recent representative examples include: a) M. Carboni, M. Clémancey, F. Molton, J. Pécaut, C. Lebrun, L. Dubois, G. Blondin and J.-M. Latour, *Inorg. Chem.* 2012, **51**, 10447. b) S. J. Tereniak, R. K. Carlson, L. J. Clouston, V. G. Young, Jr., E. Bill, R. Maurice, Y.-S. Chen, H. J. Kim, L. Gagliardi and C. C. Lu, *J. Am. Chem. Soc.,* 2014, **136**, 1842. c) Y. Sano, N. Lau, A. C. Weitz, J. W. Ziller, M. P. Hendrich and A. S. Borovik, *Inorg. Chem.,* 2017, **56**, 14118.
6 A. Nicolay and T. D. Tilley, *Chem. Eur. J.,* 2018, **24**, 10329.
7 A. N. Desnoyer, A. Nicolay, P. Rios, M. S. Ziegler and T. D. Tilley, *Acc. Chem. Res.,* 2020, **53**, 1944.
8 a) A. S. Borovik, L. Que, Jr., V. Papaefthymiou, E. Münck, L. F. Taylor and O. P. Anderson, *J. Am. Chem. Soc.,* 1988, **110**, 1986. b) T. R. Holman, Z. Wang, M. P. Hendrich and L. Que, Jr., *Inorg. Chem.,* 1995, **34**, 134.
9 A. L. Poptic, Y.-P. Chen, T. Chang, Y.-S. Chen, C. E. Moore and S. Zhang, *J. Am. Chem. Soc.,* 2023, **145**, 3491.
10 a) U. Bossek, T. Weyhermüller, K. Wieghardt, J. Bonvoisin and J. J. Girerd, *J. Chem. Soc., Chem. Commun.* 1989, 633. b) R. Hotzelmann, K. Wieghardt, U. Floerke, H. J. Haupt, D. C. Weatherburn, J. Bonvoisin, G. Blondin and J. J. Girerd, *J. Am. Chem. Soc.,* 1992, **114**, 1681.
11 J. L. Lee, S. Biswas, J. W. Ziller, E. L. Bominaar, M. P. Hendrich, A. S. Borovik, *Chem. Sci.* **2024**, *15*, 2817.
12 a) C. He and S. J. Lippard, *Tetrahedron*, 2000, **56**, 8245 b) C. He and S. J. Lippard, *J. Am. Chem. Soc.,* 2000, **122**, 184.
13 a) R. Ziessel, J. Suffert and M.-T. Youinou. *J. Org. Chem.,* 1996, **61**, 6535. b) J. Y. Hwang, H.-G. Jeon, Y. R. Choi, J. Kim, P. Kang, S. Lee and K.-S. Jeong, *Org. Lett.,* 2017, **19**, 5625.
14 L. Yang, D. R. Powell and R. P. Houser, *Dalton Trans.,* 2007, 955.
15 For studies on related bimetallic complexes, see for example S. M. Bellows, N. A. Arnet, P. M. Gurubasavaraj, W. W. Brennessel, E. Bill, T. R. Cundari, P. L. Holland, *J. Am. Chem. Soc.* **2016**, *138*, 12112.

The data supporting this article have been included as part of the Supplementary Information.

CCDC 2349134-2349138 contain the supplementary crystallographic data for this paper. These data can be obtained free of charge *via* www.ccdc.cam.ac.uk/dat_request/cif, or by emailing data_request@ccdc.cam.ac.uk, or by contacting the Cambridge Crystallographic Data Centre, 12 Union Road, Cambridge CB2 1EZ, UK; fax: +44 1223 336033